Applied Catalysis B: Environmental 166–167 (2015) 217–223

Contents lists available at ScienceDirect

Applied Catalysis B: Environmental

journal homepage: www.elsevier.com/locate/apcatb

Preparation of 3D reticulated ZnO/CNF/NiO heteroarchitecture for high-performance photocatalysis

Chengzhi Luo[a], Delong Li[a], Wenhui Wu[a], Chaozhi Yu[a], Weiping Li[a], Chunxu Pan[a,b,*]

[a] School of Physics and Technology, and MOE Key Laboratory of Artificial Micro- and Nano-structures, Wuhan University, Wuhan 430072, China
[b] Center for Electron Microscopy, Wuhan University, Wuhan 430072, China

ARTICLE INFO

Article history:
Received 14 September 2014
Received in revised form 7 November 2014
Accepted 15 November 2014
Available online 21 November 2014

Keywords:
Three-dimensional
Reticulated
ZnO/CNF/NiO
Heteroarchitecture
Photocatalysis.

ABSTRACT

In this paper, we introduce a novel facile two-step chemical vapor deposition (CVD) route as a straightforward protocol for preparing a kind of three-dimensional (3D) reticulated ZnO/CNF/NiO heteroarchitectured composite. In the experiment, carbon nanofibers (CNFs) grew directly on porous Ni foam, and ZnO nanorods were seamlessly and uniformly grew from CNFs. The experimental results revealed this composite an excellent photocatalytic performance 2.5 times higher than that of regular ZnO/NiO composite. This is because of the following advantages: the 3D reticulated structure provides more nucleation sites for ZnO nanorods, in which the light would be reflected multiply and thus increased the absorption efficiency of the light; because CNFs formed two strong and compact hetero-interfaces with both ZnO nanorods and NiO substrate, respectively, it provided barrier-free access to transport photo-induced carriers (electrons and holes) between ZnO and NiO as bridge during photocatalytic process, which therefore greatly improved the separation efficiency of the electrons and holes. It is expected that the 3D heteroarchitectured composite will have potential applications in the areas of environmental improvement, green energy, water splitting, hydrogen generation, etc.

1. Introduction

Environmental pollution including organic pollutants and toxic water pollutants has become a world-wide problem, along with the industrial development. In recent years, photocatalytic technology has attracted a great attention, due to its advantages such as thorough pollutant purification, nontoxicity, strong oxidation and reduction, long-term stability, high degradation efficiency, etc [1]. In general, most photocatalysts are metal oxides or semiconductors, such as TiO_2 [2], ZnO [3], Bi_2O_3 [4], CdS [5], etc. Among these photocatalysis, TiO_2 and ZnO have been recognized as the excellent materials for photocatalysis because of their high photosensitivity, nontoxic nature and large band gap [6,7]. Compared with TiO_2, ZnO belongs to a direct wide bandgap n-type semiconductor with a bandgap of 3.2 eV closing to TiO_2, and it has advantages involving high chemical and thermal stability, high photosensitivity, high catalytic activity, suitable bandgap, nontoxic, low cost and environmental friendliness. In addition, researchers have revealed that the quantum efficiency and photocatalytic efficiency of ZnO are higher than that of TiO_2, which makes ZnO a promising photocatalyst [8].

However, improving the photocatalytic efficiency of ZnO to meet practical application requirements is still a challenge, because of the bottleneck of poor quantum yield caused by rapid recombination of the photo-induced electrons and holes [9]. In order to reduce the recombination of the electron–hole pairs, several attempts have been made for ZnO modification, such as metal and non-metal ion-doping, noble metal deposition, oxide semiconductor coupling and so on [10–13]. Generally, oxide semiconductor coupling is one of an effective process, which enhances the light utilization efficiency and the electron–hole pair separation efficiency via forming a heterojunction between two different oxide semiconductors.

In different coupling system, ZnO/NiO composite is the most concerned [14]. NiO has been under extensive investigation due to its interesting electronic structure, strongly affected by Ni 3d electrons, which are localized in space but spread out over a wide energy range because of strong coulomb repulsion between them. Being a p-type semiconductor (E_g = 3.5 eV) with rock salt or cubic structure, NiO has wide technological applications, based on its electrical, magnetic and optical properties for magneto-resistance sensors, electrochromic devices, transparent conducting films and chemical sensors [15]. In addition, Ni foam is highly porous structured material with large specific surface area and good processing performance, which can be used as a template for preparing 3D reticulated composite to further improve energy utilization rate.

* Corresponding author. Tel.: +86 27 68752481 ext 8168.
E-mail address: cxpan@whu.edu.cn (C. Pan).

http://dx.doi.org/10.1016/j.apcatb.2014.11.030
0926-3373/

In our previous work, ZnO and Ni foam were used to fabricate porous micro-nanostructure NiO/ZnO composite, which exhibited improved photocatalytic properties [14].

It is well known that one-dimensional carbon nanofibers (CNFs) have been widely used as ideal electron pathways due to their good conductivity ($\rho = (3–7) \times 10^{-3}\ \Omega\,cm$) [16]. Some results have demonstrated that CNFs could efficiently capture and transport photo-induced electrons through highly conductive long CNFs. More importantly, one of the attractive features of CNFs is that the nanofibers can be readily prepared as materials with favorable recycling characteristics [17].

Judging from the excellent photocatalyst of ZnO/NiO composite and the efficient electron transfer property of CNFs, the combination of ZnO/NiO composite and CNFs seems to be ideal for hindering the recombination of electrons and holes and improving the photocatalytic efficiency. At present, CNFs were generally composited with oxide semiconductors via hydrothermal methods [18,19]. However, it is difficult to form a strong and closely connected heteroarchitecture, or merely mechanical contact with "gaps" at the interface, when using hydrothermal methods at low temperature, which will impede the electron transportation, and also affect the stability and service life of the composites [20].

In this paper, we reported a simple two-step chemical vapor deposition (CVD) route to fabricate a kind of 3D reticulated ZnO/CNF/NiO heteroarchitectured composite. In the experiment, CNFs grew directly on porous Ni foam, and ZnO nanorods were seamlessly and uniformly grew from CNFs. The experimental results revealed this composite an excellent photocatalytic performance 2.5 times higher than that of regular ZnO/NiO composite. This is because of the following advantages: (1) The 3D reticulated structure of CNFs provided more nucleate sites for ZnO nanorods, in which the light could be multiply reflected, and increased the light utilization rate; (2) During two-step CVD process, a strong and closely contacted interface was formed between ZnO nanorods and CNFs, and CNFs and NiO film, respectively, which facilitated the mobility ratio of the photo-induced carriers. During photocatalytic process, CNFs acted as bridges to transport electrons and holes between ZnO and NiO, which further improved the separation efficiency of the electrons and holes, and enhanced the photocatalytic property.

2. Experimental

The syntheses of the ZnO/CNF/NiO composite via two-step CVD process: (1) growing CNFs on the Ni foam substrate by using a thermal CVD. The Ni foam was placed in a quartz tube reactor and 200 sccm Ar was continuously introduced into the quartz tube. CNFs grew on the porous Ni foam by adding 10 sccm C_2H_2 at 700 °C for 10 min; (2) growing ZnO nanorods on CNFs. Zn powder (99.99%) was placed in a quartz boat located inside a quartz tube. The as-grown CNF/Ni composite was placed on the downstream of the quartz tube. The temperature of the reactor was maintained at 600 °C. The growth time was 1 h. Argon was injected into the tube from the start of heating constantly with a rate of 500 sccm. The residual oxygen was incorporated into growth of the ZnO nanorods and oxidation of Ni foam. As a comparative experiment, the pure Ni foam was used to prepare ZnO/NiO composite with equal ZnO content in the second CVD process. Fig. 1 illustrates the schematic diagram for preparing the ZnO/CNF/NiO heterostructure composite.

The morphology and microstructure of the samples were characterized using a scanning electron microscope (SEM; S-4800 HITACHI, Japan) and high-resolution transmission electron microscopy (HRTEM; JEM 2010FEFHRTEM, JEOL, Japan). X-ray diffraction patterns were recorded on an X-ray diffractometer

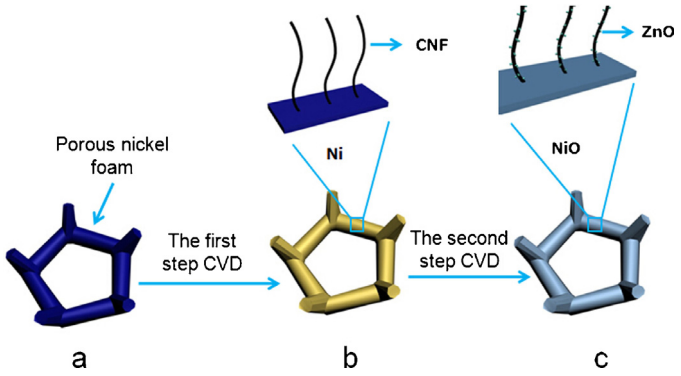

Fig. 1. Schematic diagram for preparing the ZnO/CNF/NiO heterostructure composite by using a two-step CVD process: (a) original Ni foam; (b) growing CNFs upon Ni foam via the first CVD process; (c) growing ZnO nanorods upon CNFs and transformation of Ni foam surface into NiO via the second CVD process.

(XRD; D8 Advance, Bruker AXS, Germany) for phase characterization. Chemical compositions and chemical environment of the carbon atoms were analyzed by using an X-ray photoelectron spectroscopy (XPS; AXIS-Ultra instrument, Kratos Analytical, England) with monochromatic Al Kα radiation (225 W, 15 Ma, 15 kV). UV–vis diffuse reflectance spectra (DRS) of the samples were measured by using a diffuse reflectance accessory of UV–vis spectrophotometer (UV-2550; Shimadzu, Kyoto, Japan). The photocurrents were measured by an electrochemical workstation (CHI 660C, China) in 0.1 M Na_2SO_4 aqueous solution at room temperature.

The photoreactor was designed with an internal light source surrounded by a quartz jacket (450 W high-pressure mercury lamp with main emission wavelength of 313 nm), 100 mL of the rhodamine B (RB) solution, with an initial concentration of 10 mg/L, was used in the presence of the solid catalyst (0.035 g). The solution was stirred in the dark for 30 min to obtain a good dispersion and to reach the adsorption–desorption equilibrium between the organic molecules and the catalyst surface. Decreases in the concentration of the dye were analyzed by a UV–vis spectrophotometer (UV-2550; Shimadzu, Kyoto, Japan) at $\lambda = 553$ nm. At given intervals of illumination, samples of the reaction solution were taken out and analyzed.

3. Results and discussion

Fig. 2 shows the SEM images of CNFs growing directly on Ni foam. Obviously, the pristine Ni foam was of a 3D porous structure, and the entangled dense CNFs were well distributed on the surface of Ni foam framework with a size of 100 nm in diameter and 20–50 μm in length. Comparing with CNFs growing on a flat surface, the present CNFs made full use of the large internal surface of Ni foam. In addition, CNFs exhibited a strong and close contact with Ni foam, because CNFs were growing directly on the Ni foam. Fig. 3 shows the SEM morphologies of the ZnO/CNF/NiO composite. It could be seen that the dense and homogeneous hexagonal ZnO nanorods were developed from CNFs with 10–20 nm in diameter and about 200 nm in length. It is worth to note that CNFs with large specific surface area provided more nucleate sites for the ZnO nanorod growth. Therefore, the ZnO nanorods grew vertically upon CNFs and formed a close and compact contact with CNFs.

Fig. 4 illustrates the XRD patterns of the CNF/Ni and ZnO/CNF/NiO composites. Obviously, for the first CVD process, only the peaks of Ni and CNFs were indexed, while the peaks of ZnO, NiO and Ni were obtained after the second CVD process, which indicated that the thermal evaporated Zn had been transformed into ZnO nanorods completely and part of Ni foam had been oxidized into NiO film.

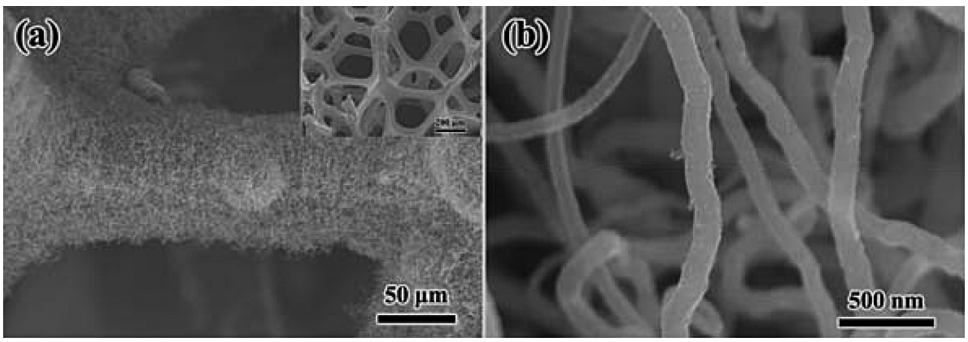

Fig. 2. SEM morphologies of as-prepared CNFs grown upon Ni foam: (a) low magnification; inset shows the pristine Ni foam; (b) high magnification.

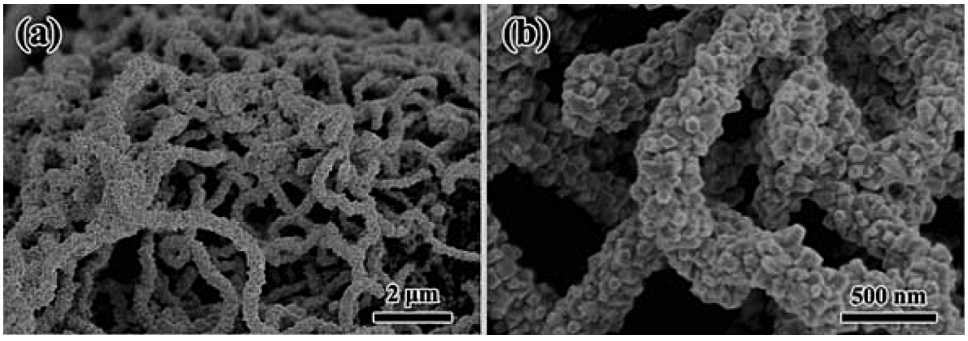

Fig. 3. SEM morphologies of the ZnO/CNF/NiO composite: (a) low magnification; (b) high magnification.

Figs. 5 show the XPS spectra of the ZnO/CNF/NiO composite. From the fully scanned spectrum in the range of 0–1200 eV, only C, O, Zn and Ni elements were detected. Fig. 6a is the high-resolution XPS spectra for the C 1s region around 285 eV, in which the binding energy peak at 284.6 eV was attributed to the amorphous carbon phase or from adventitious carbon, the peak at 285.6 eV was the characteristic peak of the combination of C–C bands [18], and the peak at 283.9 eV is characteristic peak of Ni–C compounds which suggested that the Ni foam acted as nucleation sites for growing CNFs [21]. Fig. 6b presents the spectrum of O 1s. The asymmetric and wide peak of the O 1s spectrum demonstrated that there was more than one chemical state according to the binding energy. That was to say, the peaks at 529.7, 530.6 and 528.1 eV related to Ni–O, Zn–O and surface hydroxyl groups (O–H) [22,23]. Fig. 6c shows two symmetric peaks of the Zn 2p spectrum. The peak centered at 1021.9 eV corresponded to Zn 2p3/2, while the peak at 1044.9 eV was assigned to Zn 2p1/2, which indicated a normal state of Zn 2p in the ZnO/CNF/NiO composite [18]. Fig. 6d illustrates Ni 2p spectrum. The peaks at 854.7 and 860.4 eV belonged to Ni-O bonding, and the peaks at 852.8 and 859.4 eV were pure Ni [22], which was similar to XRD results. All of these XPS results indicated that the ZnO/CNF/NiO composites were composed of the phases of ZnO, CNF and NiO.

Up to now, there have been many researches on the growth of CNFs upon porous Ni foam [24]. In order to understand the growth mechanism of the ZnO/CNF/NiO heteroarchitectures, we concentrated our study on the ZnO growth on CNFs. Fig. 7 shows the SEM morphologies of ZnO nanorods grew upon CNFs with different thermal evaporation time. Obviously, with time increased, the number of ZnO nanorods was increased. When the time extended to 40 min, ZnO nanorods had fully covered CNFs. Therefore, we propose a "nucleation and growth model" for explaining the growth mechanism of ZnO nanorods upon CNFs. That is: (1) Zn powders were thermally evaporated at high temperature and reacted with oxygen; (2) The ZnO vapor flowed into the low-temperature zone and deposited upon the CNFs surface to form a small crystal nuclei; (3) With the time increasing, ZnO crystal nucleus would gradually grow into a typical hexagonal rod structure. At the same time, more and more ZnO deposited on CNFs until it was completely covered.

In fact, the purpose of present work was to obtain two strong and close contact interfaces of ZnO nanorods/CNFs and CNFs/NiO film

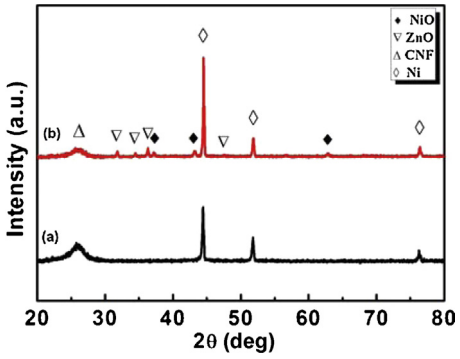

Fig. 4. XRD patterns of the composites: (a) CNF/Ni, (b) ZnO/CNF/NiO.

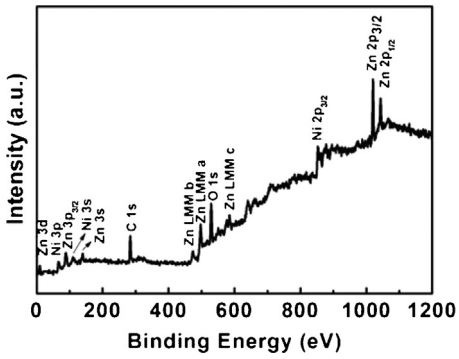

Fig. 5. Fully scanned XPS spectra of the ZnO/CNF/NiO composite.

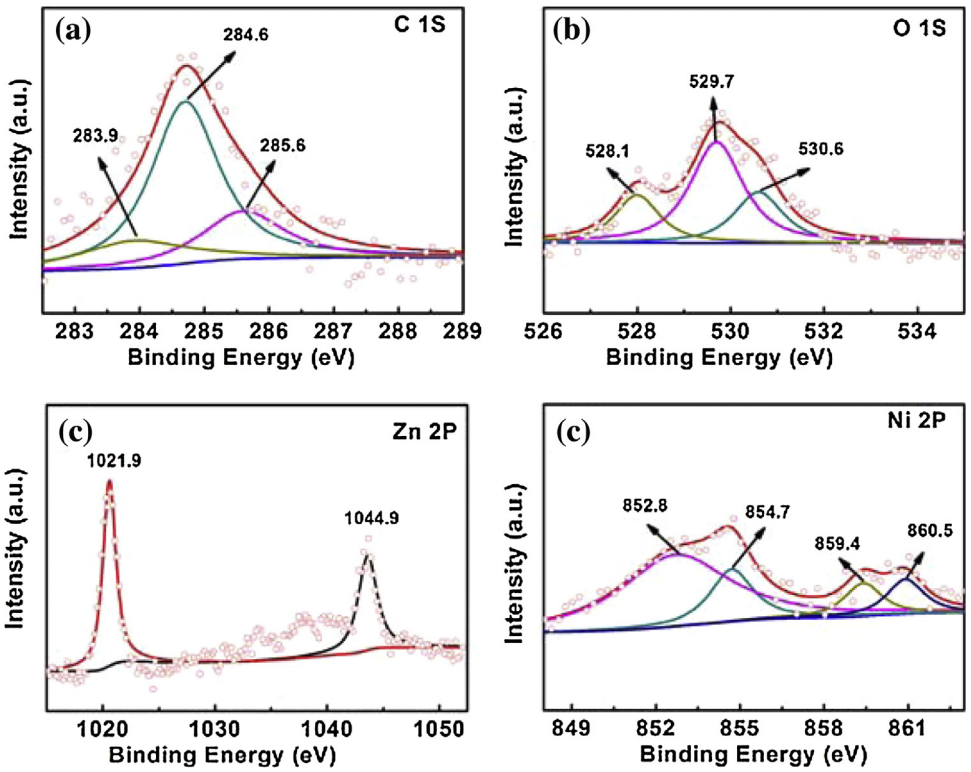

Fig. 6. XPS spectra of the ZnO/CNF/NiO composite: (a) C 1s scan, (b) O 1s scan, (c) Zn 2p scan, (d) Ni 2p scan.

for ensuring smooth transfer of the photo-induced carriers (electrons and holes), increase the physical and chemical properties of the ZnO/CNF/NiO composite and also improve the stability during long-term service. In general, although a NiO/ZnO composite can be obtained from chemical method at low temperature and also exhibits an epitaxial growth, it was difficult to form strong and close contact, but merely mechanical contact with "gaps" at the interface, which has negative effect on the performance and stability of the composite.

It has been known that there was a close contact between CNFs and Ni foam when CNFs were grown directly on porous Ni foam [24]. In the present work, the interface between ZnO and CNFs of the ZnO/CNF/NiO composite was observed by using TEM and HRTEM, as shown in Fig. 8. Obviously, there was a compact

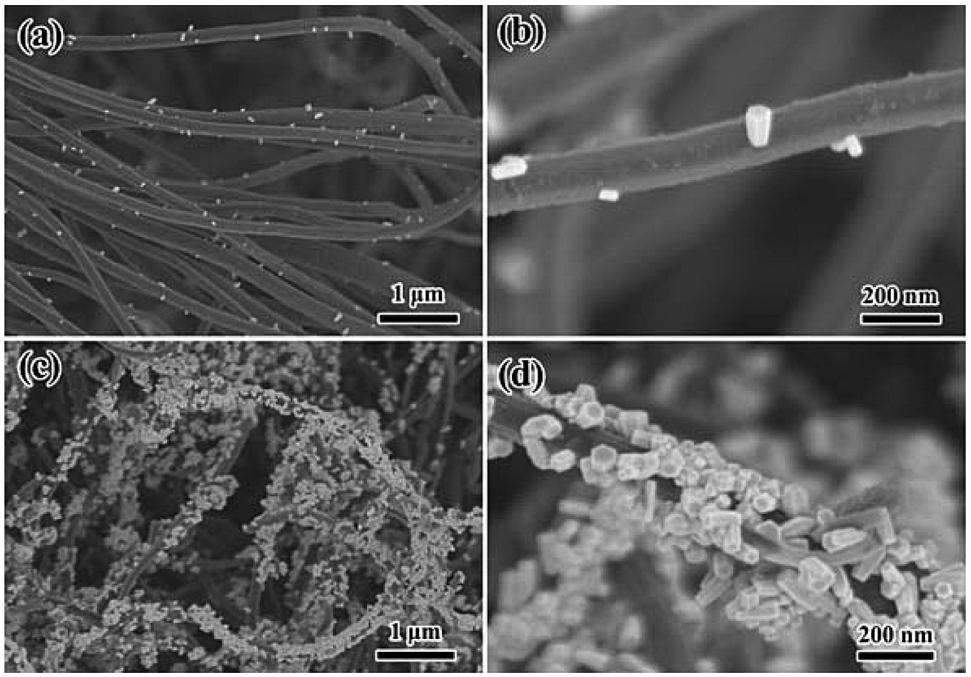

Fig. 7. SEM morphologies of ZnO nanorods grew upon CNFs with different thermal evaporation time: (a) 20 min; (b) 20 min (high magnification); (c) 40 min; (d) 40 min (high magnification).

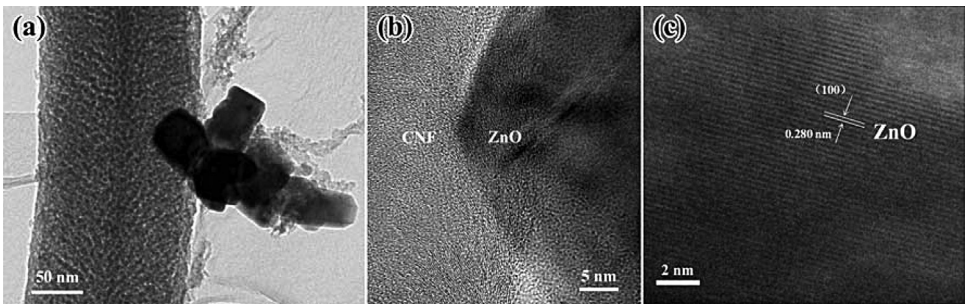

Fig. 8. TEM and HRTEM micrographs of ZnO nanorods grew upon CNFs: (a) TEM image; (b) HRTEM image of the interface between ZnO nanorod and CNF; (c) HRTEM image of ZnO nanorod.

combination interface between ZnO nanorod and CNF. That is to say, during thermal evaporation, ZnO was seamlessly deposited on the CNFs surface and directly grew from CNFs. This compact contacted interface provided a barrier-free access for the carrier (electrons or holes), which played an important role for improving the physical and chemical properties of the ZnO/CNF/NiO composite.

Fig. 9 illustrates the UV–vis diffuse reflectance spectra (DRS) of the ZnO/CNF/NiO and ZnO/NiO composites. The strong absorption in the visible range of the ZnO/CNF/NiO composite was caused by the CNFs and had no contribution to the generation of electrons and holes [6]. Regardless of the effect of the CNFs, the experimental results revealed that the ZnO/CNF/NiO composite exhibited a strong absorption for UV light, when compared with ZnO/NiO. It is expected to have a positive impact on enhancing its photocatalytic properties.

Photocurrent measurement generally is used for investigating the separation efficiency of photo-induced carriers (electron or holes), and the photocurrent responses were performed via shading and not shading the light irradiation. In the photocurrent measurement, a three-electrode system was used, i.e., a saturated calomel electrode (SCE) was used as the reference electrode; and the prepared samples (1×1 cm) and a platinum wire were used as the working electrode and counter electrode, respectively. Fig. 10 gives the photocurrent density spectra of the ZnO/CNF/NiO, CNF/Ni and ZnO/NiO composites. Obviously, all composites possessed fast and uniform photocurrent responses, which were entirely reversible. However, under the UV–vis light irradiation, the photocurrent density of the CNF/Ni was almost invisible, while the photocurrent density of the ZnO/CNF/NiO composite reached to as high as 3.0 μA/cm^2, which was three times higher than that of the ZnO/NiO composite. This enhancement demonstrated the importance of CNFs on the synergetic effect in the ZnO/CNF/NiO composite, which greatly improved separation efficiency of the photo-induced electrons and holes.

In order to evaluate the photocatalytic activity of the ZnO/CNF/NiO composite, the experiment of degradation for RB solution was carried out under the UV–vis light irradiation. For comparison, the samples including CNF/Ni, ZnO/NiO and mechanically mixed NiO with CNF/ZnO (denoted as NiO + CNF/ZnO) were also used as photocatalytic references, as shown in Fig. 11. The concentration variation of RB solution was represented from the spectrum strength of the absorption for the UV–vis light irradiation. The degradation efficiency was defined as $(C_0 - C)/C_0$, where C_0 and C were the initial and remnant concentrations of RB, respectively. Before the tests of photocatalytic activities, the two control experiments were performed under different conditions: (1) in the presence of the photocatalysts but in the dark; (2) under the UV–vis light irradiation but in the absence of the photocatalysts, as observed in Fig. 11a. These control experiments showed that the adsorption–desorption equilibrium of RB in the dark was established within 30 min, and there was no appreciable degradation of RB in the absence of the photocatalysts. Fig. 11b shows the degradation curves of RB when using different samples. It could be seen that CNF/Ni exhibited negligible activity, while the ZnO/CNF/NiO composite had the highest photocatalytic activity. Generally, after 2 h of reaction, the degradation efficiency of four samples reached 98, 85, 68 and 14%, respectively.

When the initial concentration of the reactant was low (10 mg/L for the present test), the above degradation reactions followed a Langmuir–Hinshel–wood apparent first-order kinetics model [25], which was:

$$\ln \frac{C}{C_0} = -kKt = -k_{app}t$$

where t is the irradiation time (min), k is the degradation rate of the reactant (mg/(L min)), K is the adsorption coefficient of the reactant (L/mg) and k_{app} is the apparent first-order rate constant (min^{-1}). Therefore, the photocatalytic activity of the catalysts could be determined from the k_{app} values.

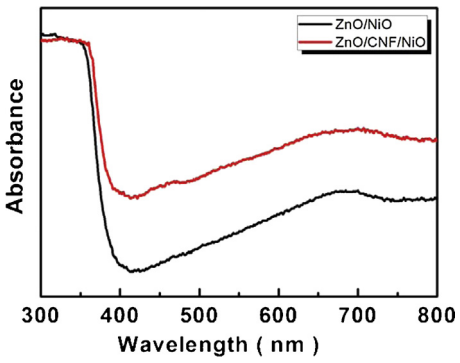

Fig. 9. UV–vis diffuse reflectance spectra of the composites.

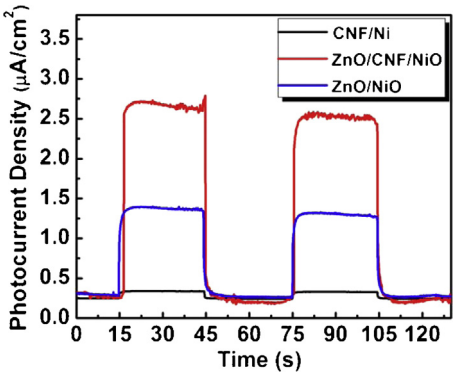

Fig. 10. Photocurrent density spectra of the composites.

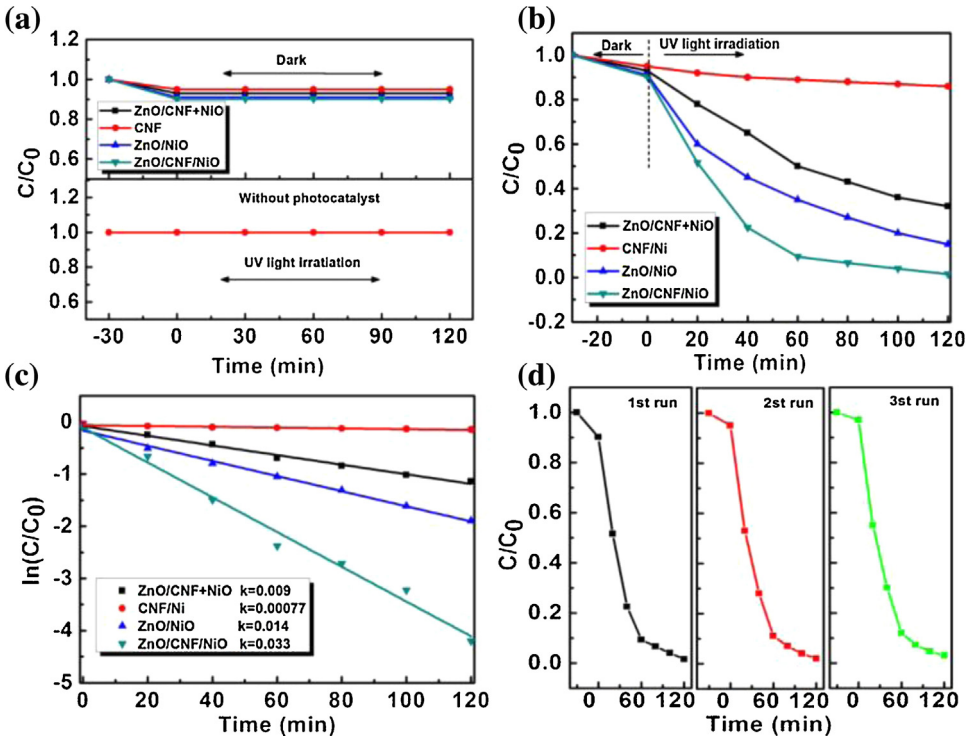

Fig. 11. Photocatalytic property of the composites for degradation of RB solution: (a) degradation profiles of RB in the presence of photocatalysts in dark and in the absence of photocatalysts with light irradiation; (b) degradation profiles of RB photocatalytic degradation; (c) kinetic linear simulation curves of RB photocatalytic degradation; (d) photocatalytic activity of the ZnO/CNF/NiO for RB degradation with three times cycling.

According to Fig. 11c, the photocatalytic activity order was ZnO/CNF/NiO > ZnO/NiO > NiO + CNF/ZnO > CNF/Ni.

Moreover, property stability was also a crucial factor for the ZnO/CNF/NiO composite when it was applied in environmental service. Fig. 11d gives the degradation curves of RB for three cycles. Obviously, the photocatalytic activity of the ZnO/CNF/NiO composite remained almost unchanged.

Based on the above results, a proposed mechanism was being discussed to explain the enhancement of the photocatalytic properties of the ZnO/CNF/NiO composite which was similar to the literatures [17,18]. The mechanism was that the high photocatalytic activity of the ZnO/CNF/NiO composite was mainly attributed to the bridge effect of CNFs in facilitating the separation efficiency of electrons and holes. Under UV light irradiation, both ZnO and NiO absorbed the photons. The high-energy photon excites an electron from the valence band (VB) to the conduction band (CB) of ZnO and NiO. Because the CB levels of ZnO and NiO are located significantly higher than the Fermi level of CNFs, photogenerated electrons in ZnO and NiO would move freely to the surface of the CNFs; meanwhile, the photogenerated holes were left in the VB of ZnO and NiO. The holes were ultimately trapped by surface hydroxyl groups (or H_2O) at the catalyst surface to yield OH• radicals, which was a strong oxidizing agent to decompose the organic dye. The dissolved oxygen molecules reacted with the surface of the CNFs electrons to yield superoxide radical anions, $O2•^-$, which on protonation generated the hydroperoxy, HO_2•, radicals, producing hydroxyl radical OH•. Furthermore, the better separation of photogenerated electrons and holes in the ZnO/CNF/NiO composite was confirmed by photocurrent as shown in Fig. 10. The efficient charge separation could increase the lifetime of the charge carriers and enhance the efficiency of the interfacial charge transfer to adsorbed substrates and then account for the higher activity of the ZnO/CNF/NiO composite photocatalyst. On the other hand, the 3D reticulated structure provides more nucleation sites for ZnO nanorods, in which the light would be reflected multiply and thus improved the absorption efficiency of the light.

4. Conclusions

In summary, the 3D reticulated ZnO/CNF/NiO composite was prepared via a two-step CVD process. It exhibited the unique features, i.e., the substrate was Ni foam covered with a NiO film, CNFs grew directly on Ni foam and the ZnO nanorods were formed on CNFs. In this composite, CNF has two strong and compact heterointerfaces with both NiO film and ZnO nanorod, which greatly improved the separation efficiency of the photo-induced carriers (electron and holes) and also the structural stability of the composite. This process has advantages involving simple, fast and cost-effective. In addition to the photocatalysis, it is expected to have potential application prospect in green energy, water splitting and hydrogen generation, supercapacitors, field emission, and micro-nano devices, etc.

Acknowledgments

This work was supported by the National Nature Science Foundation of China (Nos. 11174227, 51209023, J1210061), National Key Technology R&D Program of the Hubei province (No. 2013BHE012), National Basic Research Program of China (973 Program) (No. 2009CB939705) and Chinese Universities Scientific Fund.

References

[1] M.R. Hoffmann, S.T. Martin, W. Choi, D.W. Bahnemann, Chem. Rev. 95 (1995) 69.
[2] Q. Wu, R. Krol, J. Am. Chem. Soc. 134 (2012) 9369.
[3] C. Tian, Q. Zhang, A. Wu, M. Jiang, Z. Liang, B. Jiang, H. Fu, Chem. Commun. 48 (2012) 2858.

[4] X. Xiao, R. Hu, C. Liu, C. Xing, C. Qian, X. Zuo, J. Nan, L. Wang, Appl. Catal. B 140–141 (2013) 433.
[5] S. Wang, X. Wang, Appl. Catal. B 162 (2015) 494.
[6] D. Li, Y. Zhang, W. Wu, C. Pan, RSC Adv. 4 (2014) 18186.
[7] J. Xie, H. Wang, M. Duan, L. Zhang, Appl. Surf. Sci. 257 (2011) 6358.
[8] L. Yang, S. Dong, J. Sun, J. Feng, Q. Wu, S. Sun, J. Hazard Mater. 179 (2010) 438.
[9] Z. Zhang, C. Shao, X. Li, L. Zhang, H. Xue, C. Wang, Y. Liu, J. Phys. Chem. C 114 (2010) 7920.
[10] D. Zhang, F. Zeng, J. Mater. Sci. 47 (2012) 2155.
[11] A.P. Bhirud, S.D. Sathaye, R.P. Waichal, L.K. Nikam, B.B. Kale, Green Chem. 14 (2012) 2790.
[12] R. Georgekutty, M.K. Seery, S.C. Pillai, J. Phys. Chem. C 112 (2008) 13563.
[13] D. Li, X. Jiang, Y. Zhang, B. Zhang, C. Pan, J. Mater. Res. 177 (2012) 1.
[14] C. Luo, D. Li, W. Wu, Y. Zhang, C. Pan, RSC Adv. 4 (2014) 3090.
[15] A. Hameed, T. Montini, V. Gombaca, P. Fornasiero, Photochem. Photobiol. Sci. 8 (2009) 677.
[16] H.E. Unalan, D. Wei, K. Suzuki, S. Dalal, P. Hiralal, H. Matsumoto, S. Imaizumi, M. Minagawa, A. Tanioka, A.J. Flewitt, W.I. Milne, G.A.J. Amaratunga, Appl. Phys. Lett. 93 (2008) 133116.
[17] M. Zhang, C. Shao, J. Mu, X. Huang, Z. Zhang, Z. Guo, P. Zhang, Y. Liu, J. Mater. Chem. 22 (2012) 577.
[18] J. Mu, C. Shao, Z. Guo, Z. Zhang, M. Zhang, P. Zhang, B. Chen, Y. Liu, ACS Appl. Mater. Interf. 3 (2011) 590.
[19] C. Li, Y. Zhang, M. Mann, P. Hiralal, H.E. Unalan, W. Lei, B.P. Wang, D.P. Chu, D. Pribat, G.A.J. Amaratunga, W.I. Milne, Appl. Phys. Lett. 96 (2010) 143114.
[20] D. Eder, Chem. Rev. 110 (2010) 1348.
[21] S. Sinharoy, L.L. Levenson, Thin Solid Films 53 (1978) 31.
[22] M. Caffio, B. Cortigiani, G. Rovida, A. Atrei, C. Giovanardi, J. Phys. Chem. B 108 (2004) 9919.
[23] J. Liu, X. Li, L. Dai, Adv. Mater. 18 (2006) 1740.
[24] J.K. Chinthaginjala, K. Seshan, L. Lefferts, Ind. Eng. Chem. Res. 46 (2007) 3968.
[25] M.S. Lee, S.S. Park, G. Lee, C. Ju, S. Hong, Catal. Today 101 (2005) 283.